Rubisco activase remodels plant Rubisco via the large subunit N-terminus

Jediael Ng and Oliver Mueller-Cajar*

School of Biological Sciences, Nanyang Technological University, 60 Nanyang Drive, Singapore 637551. Singapore

*Correspondence: cajar@ntu.edu.sg

Running title: Mechanism of Rubisco activase

Author Contributions

J. N. designed research and performed the experiments. J. N. and O.M.-C. wrote the article.

KEYWORDS

Rubisco, Rubisco activase, ATPases associated with diverse cellular activities (AAA), photosynthesis, molecular chaperone, carbon fixation

ABSTRACT

The photosynthetic CO_2 fixing enzyme ribulose 1,5-bisphosphate carboxylase/oxygenase (Rubisco) forms inhibited complexes with multiple sugar phosphates, including its substrate ribulose 1,5-bisphosphate. At least three classes of ATPases associated with diverse cellular activities (AAA+ proteins) termed Rubisco activases (Rcas) have evolved to remodel inhibited Rubisco complexes. The mechanism of green-type Rca found in higher plants has proved elusive, because until recently higher plant Rubiscos could not be expressed recombinantly. Towards identifying interaction sites between Rubisco and Rca, here we produce and characterize a suite of 33 Arabidopsis Rubisco mutants for their ability to be activated by Rca. We find that Rca activity is highly sensitive to truncations and mutations in the conserved N-terminus of the Rubisco large subunit. Both T5A and T7A substitutions cannot be activated by Rca, but present with increased carboxylation velocities. Our results are consistent with a model where Rca functions by transiently threading the Rubisco large subunit N-terminus through the axial pore of the AAA+ hexamer.

INTRODUCTION

Virtually all carbon dioxide that enters the biological world does so via the Calvin Benson Bassham cycle (1). Aerobic autotrophic organisms such as plants, algae and cyanobacteria all utilize this somewhat suboptimal CO_2-fixation process, which is dependent on catalysis by the slow and promiscuous enzyme Rubisco. The enzyme binds the five carbon sugar Ribulose 1,5-bisphosphate (RuBP), adds a carbon dioxide molecule and hydrolyzes the six carbon intermediate to form two molecules of 3-phosphoglycerate (3PGA). In plants each active site only processes ~1-3 reactions per second, and frequently oxygen gas is incorporated instead of CO_2, which leads to production of the toxic metabolite 2-phosphoglycolate.

To overcome these flux limitations, Rubisco is overexpressed to constitute up to 50% of the leaf soluble protein and is believed to be the most abundant protein on earth (2,3). Recognition that the enzyme catalyzes the rate limiting step have made its performance the heartpiece of multiple ongoing crop improvement strategies (4,5). In addition to its slow speed and inaccuracy, the enzyme is also susceptible to form dead-end inhibited complexes with several sugar phosphates that are present in its environment (6,7). CO_2 fixation ceases, unless the inhibitors are constantly removed. This action is performed by a group of dedicated molecular chaperones that have been termed the Rubisco activases (Rcas) (8-10). Three classes of Rca exist, and although all belong to the superfamily of AAA+ proteins, their primary sequences and mechanisms are highly distinct, indicating convergent evolution(11,12). Red-type Rca found in red-lineage phytoplankton and proteobacteria transiently threads the C-terminus of the Rubisco large subunit through the axial pore of the AAA+ hexamer (13-15). In contrast the CbbQO-type Rca found in chemoautotrophic proteobacteria consists of a cup-shaped AAA+ hexamer ($CbbQ_6$) bound to a single adaptor protein CbbO, which is essential for Rubisco activation (9). During Rca function the hexamer remodels CbbO, which is bound to inhibited Rubisco via a von Willebrand Factor A domain(16).

The detailed molecular mechanism by which inhibitory compounds are removed by higher plant Rca-mediated modelling of Rubisco's active site has long remained elusive (11,17). As functional Rca could be produced recombinantly, a large volume of biochemical information has accumulated on Rca

62 variants (18,19). In summary the data supports a canonical AAA+ pore-loop threading mechanism
63 where the flat top surface of the hexameric disc engages Rubisco, followed by axial pore-loop
64 threading of an element of Rubisco(20,21). The intrinsically disordered N-terminal domain, especially
65 a conserved tryptophan, is also important in engaging the holoenzyme (21,22). Regarding Rubisco,
66 early studies using green algal *Chlamydomonas* Rubisco were able to pinpoint two residues on the
67 Rubisco large subunits' βC-βD loop that contact the specificity helix (H9) of Rca (23,24). However, a
68 historical inability to produce plant Rubisco in heterologous organisms such as *Escherichia coli*
69 hampered further progress. This hurdle was recently removed (25), and here we took advantage of the
70 newly established capability to produce and biochemically characterize many plant Rubisco variants
71 for their interaction with Rca. We find that the highly conserved RbcL N-terminus is essential for Rca
72 function, with a particular importance of two threonine residues T5 and T7. This is consistent with an
73 N-terminal pore loop threading mechanism for higher plant Rca.

74

RESULTS

A surface scan of higher plant Rubisco for Rca-interacting residues

We used the recently established *E. coli* plant Rubisco expression platform (25,26) to produce a series of Arabidopsis Rubisco large subunits variants mutated in surface-localized residues in an effort to discover additional regions important for protein-protein interactions. We first tested the βC-βD loop mutations E94K and P89A as positive controls (Fig. 1*A*), as these substitutions had earlier been shown to greatly perturb the ability of Spinach Rca to activate Chlamydomonas Rubisco (27). We then assayed the fully activated holoenzyme (ECM) and the inhibited apo enzyme bound to the substrate ribulose 1,5-bisphosphate (ER) in the presence and absence of the short (Rcaβ) isoform of Arabidopsis Rca (Fig. 1*B*). Consistent with the Chlamydomonas-spinach result, the inhibited E94K variant of Arabidopsis Rubisco remained non-functional in the presence of its cognate Rca, reconfirming the importance of the N-terminal βC-βD loop in the interaction. The P89A variant, however, was activated well in this system (Fig. 1*C*), suggesting that the βC-βD loop – Rca interaction is less sensitive to mutation when using Arabidopsis proteins.

We next targeted a range of surface-localized Rubisco large subunit residues for mutagenesis (Fig. 2*A*, Fig. S2). As we have found earlier, multiple positively charged residues on the face of the Rca disc are important for its ability to activate Rubisco (21,28), and therefore the chosen mutations were biased towards probing negatively charged surface residues. This included those located in a negatively charged pocket at the dimer-dimer interface that has recently been implicated in the binding of carboxysomal Rubisco linker proteins in prokaryotic green-type Rubiscos (Fig. 2*B*)(29,30). We successfully purified 17 variants (Fig. S1), which were all able to carboxylate RuBP similarly to wild-type (Fig. 2*C*, Fig. S3). Rca assays indicated that the different variants could still be activated effectively indicating the chosen residues were not of critical importance to the Rubisco-Rca interaction (Fig. 2*C*, Fig. S3). Only K14A showed a statistically significant 52% increase in its Rca-mediated activation rate, possibly reflecting a reduced stability of the inhibited complex. Clearly the chosen single amino-acid substitutions were insufficient to disrupt the extensive protein-protein

interaction interface involved in Rubisco activation. However, attempts to produce combinations of mutations were unsuccessful either due to insolubility or non-functionality for all tested cases.

The RbcL N-terminus is essential for Rca function

The red-type Rubisco activase CbbX transiently threads the RbcL C-terminus (13-15). However, the C-terminus of green-type Rubisco large subunits is poorly conserved and is of variable length (31), indicating a distinct mechanism for green-type Rca function. In contrast, while sequences at the N-terminus of red-type Rubisco large subunits differ between species, both length and sequence of the N-terminus of higher-plant RbcL is essentially completely conserved (Fig. 3*A*). In available crystal structures, residues 8-20 of the N-terminus are ordered only when the active site is in the closed (ligand-bound) form (Fig. 3*B*). In the closed conformation, the N-terminus is positioned directly above the 60's loop that co-ordinates P1 of the substrate, with F13, K14, G16 and K18 forming interactions with multiple residues of the 60's loop (32). Coupled with evidence that residues 9-15 of Rubisco from wheat are essential for functional carboxylation activity (33), the stringent conservation of the first 8 residues suggested thus a tantalizing target for mutational analysis.

A Rubisco variant with the first seven amino-acids replaced by methionine (ΔN7) displayed 83 % of wild-type carboxylation velocity (Fig. 3*C*). However, when the ER complex was formed, Rca was unable to reactivate ΔN7 (Fig. 3*C*). This result was consistent with the notion that a higher plant Rca hexamer engages the disordered N-terminus via its axial pore loops, followed by transient threading leading to active site disruption and inhibitor release.

A dissection of the RbcL N-terminal binding motif

We then performed a detailed mutational analysis of the RbcL N-terminus, generating a series of variants that, in the ECM form were all able to carboxylate at least as well as wild-type (Fig. 4). Shortening the N-terminus by one or two amino acids (ΔN1, ΔN2) did not negatively affect Rca function. In contrast, replacing the first four amino acids with methionine (ΔN3) or deleting residues 5-7 (ΔTET) almost completely eliminated the ability of Rca to activate Rubisco (Fig 3A).

Lengthening the N-terminus by inserting two alanine residues upstream of residue 2 (M1insAA) greatly reduced Rca function by ~64 %. Changing the register of the N-terminal sequence by inserting a AAA sequence upstream of K8 (T7insAAA) in the wild-type or ΔTET variant (TET-AAA) also eliminated function. These results indicated that Rca function was highly sensitive to both length and identity of the N-terminus.

Next, we evaluated the effect of single amino acid substitutions in the N-terminal motif. Whereas E6A and K8A substitutions were well tolerated, both T5A and T7A resulted in ~70% reductions in Rca functionality. This findings indicates that the two threonine residues are likely to play an important role in the threading process, possibly via specific interactions with residues in Rca's pore-loop 1 and 2 (20,21). We also further note that the observed 2 amino acid step interval would be consistent with successive zipper-like interactions that have been described to be utilized for substrate engagement at the central pore by multiple other AAA+ proteins (34-38).

Y20 forms a hydrogen bond to E60, a key catalytic residue that interacts with K334, which is positioned at the apex of Loop 6, and thought to orient the CO_2 molecule for gas addition (39). We hypothesized that this interaction could act to disrupt the active site, when the N-terminus is displaced by Rca-threading. The Y20F Rubisco mutant had a ~73% reduced carboxylation rate, but the activation rate by Rca was increased by 39% (Fig. 4*B*). This result suggests that the Y20-E60 interaction is important for the integrity of the active site, and its loss facilitates disruption of the inhibited complex.

Quite unexpectedly, we found that multiple N-terminal variants and E94K presented with significantly enhanced carboxylation velocities (up to 53%) compared to the wild-type enzyme under the conditions used in our spectrophotometric Rubisco assay (Fig. 4A,B). This suggests that reducing the interactions of the N-terminus with the enzyme may result in faster Rubiscos. Interestingly, the fast cyanobacterial Form IB enzyme from Synechococcus PCC6301 (40) possesses a truncated N-terminus (equivalent to ΔN6) (Fig. 3*A*). In a follow-up study, it will be important to use ^{14}C-CO_2 fixation assays to accurately quantify the carboxylation kinetics (41) and the CO_2/O_2 specificity factor of the fast N-terminal variants.

DISCUSSION

The availability of *E. coli* produced recombinant higher plant Rubiscos permitted us to rapidly produce many variants and assay their capability to be engaged and activated by their cognate Rca chaperone. Mutational analysis of the holoenzyme surface indicated that Rca compatibility was not easily disrupted, with the tested variants remaining functional (Fig. 2). Arguably, inclusion of less conservative substitutions such as charge switches, could have been more informative here.

In contrast, mutagenesis of the highly conserved N-terminus resulted in multiple variants that were able to carboxylate RuBP, but could not be activated by Rca. The best described conserved mechanism of numerous AAA+ ATPases concerns the translocation of a substrate peptide through the central pore of the hexamer (42), and this is the modus operandi of the red-type Rca (13). Green-type Rca pore-loops have been shown to be critical for Rubisco activation (20,21). In addition we have long been aware of the RbcL βC-βD loop – Rca specificity helix H9 interaction (27,43,44). Assuming an axial pore loop- RbcL N-terminal threading mechanism we can now further constrain the positioning of an Rca hexameric model (20) in relation to an inhibited Rubisco structure (45). Helix 9 elements of two adjacent Rca subunits can be placed in proximity to two RbcL βC-βD loops that are located on two adjacent dimers (Fig. 5). In this configuration the N-terminal tail (missing 6 amino-acids in the structure used) is then accessible to the Rca pore. Transient threading would then result in pulling residues 13 to 20 away from the large subunit body. Disruptions of the associated van der Waal's and polar interactions (32), especially with the RbcL 60's loop, may be sufficient to trigger active site opening and inhibitor release.

An important question that remains completely unaddressed is the role of the critical Rca N-terminal domain. This disordered stretch of ~60 amino acids is not resolved in structural models, and a single amino acid substitution of W15A eliminates Rca function (21,22). It is likely involved in an additional, so far undescribed, anchoring site.

180 The model is consistent with an exquisite structural snapshot of a prokaryotic carboxysome-associated
181 green-type Rca hexamer bound to cyanobacterial Rubisco that has been communicated in a concurrent
182 Biorxiv pre-print (46). In agreement with our findings, the study also reports that an N-terminal 9-
183 amino acid truncation of the tobacco Rubisco large subunit abolishes tobacco Rca function. Green-
184 type Rubisco activation is thus an ancient, conserved process that appears to precede the primary
185 endosymbiotic event (11).

186

MATERIALS AND METHODS

Molecular biology

Plasmids pBAD33k-*At*RbcLS, p11a-*At*C60αβ/C20 and pCDFduet-*At*R1/R2/Rx/B2 enabling the production of Arabidopsis Rubisco in *E. coli* were a gift from Dr. Manajit Hayer-Hartl (25). To achieve our final construct containing the large and small subunits of Rubisco, a 6x Histidine tag was appended to the C-terminus of rbcS via the Quikchange protocol (Stratagene). Restriction free cloning of the RBS-*At*RbcLScHis cassette was utilized to insert the cassette into the multiple cloning site 1 of the pRSFDuet™-1 plasmid (Novagen). To obtain single mutants, the Quikchange protocol was applied to pRSFduet-*At*RbcLScHis. Truncations of the N-terminus were performed by PCR amplification of regions flanking the unwanted sequence. Linearized products were then phosphorylated by T4 PNK (NEB) before end to end ligation. All primers used are listed in Table S1 and protein-encoding sequences were verified by DNA sequencing.

To obtain a vector encoding *Arabidopsis thaliana* Rca (AtRcaβ), the sequence corresponding to amino acid residues 59 to 474 (Uniprot P10896) were amplified from a cDNA library of Arabidopsis with BamHI and NotI restriction sites at the 5' and 3' end respectively. The sequence was then inserted into the multiple cloning site of the pHue expression vector using the appropriate restriction sites to yield the final construct pHueAthRcaβ.

Protein Purification

Recombinant wild-type activase from Arabidopsis were expressed and purified following our protocol for the purification of *Agave tequilana* activases to yield activases with a single glycine prior to the native N-terminus of the enzyme (28). For expression and purification of recombinant Rubiscos, *E.coli* BL21 cells containing p11a-*At*C60αβ/C20, pCDFduet-*At*R1/R2/Rx/B2, and pRSFduet-*At*RbcLScHis were grown in LB medium supplemented with ampicillin (200 µg mL^{-1}), kanamycin (30 µg mL^{-1}), and streptomycin (50 µg mL^{-1}). Starter cultures of 2 mL were grown overnight at 37°C prior to inoculation of 1 L cultures. Large scale cultures were grown for 3 hours at 37°C to reach an OD600 of 0.3 - 0.4 before temperatures were lowered to 23°C and harvested after 16

hours. Cells were lysed in Histrap-buffer A (50 mM Tris-HCl pH 8.0, 50 mM NaCl, 10 mM Imidazole). Soluble fractions were then applied to HisTrap HP 5 mL columns (Sigma Aldrich) equilibrated with Histrap-buffer A. Proteins were eluted with a linear imidazole gradient from 10 mM to 200 mM. Following elution, Rubisco containing fractions were immediately subjected to a Superdex 200 gel filtration column (GE Healthcare) equilibrated with buffer A (20 mM Tris-HCl pH 8.0, 50 mM NaCl) supplemented with 5% (v/v) glycerol. Pure Rubisco fractions were then pooled, concentrated, and flash-frozen for storage at -80°C. Pure proteins were quantified my measuring their absorbance at 280 nm, using extinction coefficients calculated using the ProtParam tool (https://web.expasy.org/protparam/).

Biochemical assays

Rubisco and Rubisco reactivation activities were measured and quantified as described (14), using the spectrophotometric Rubisco assay (47). RuBP was synthesized enzymatically from ribose 5-phosphate (48) and purified by anion exchange chromatography(49). ECM was formed by incubating 20 µM Rubisco active sites in Buffer A supplemented with 20 mM $NaHCO_3$ and 10 mM $MgCl_2$ (50 mins, 25 °C). For ER, complexes were generated by incubating 20 µM Rubisco active sites in Buffer A containing 4 mM EDTA (10 mins) prior to addition of RuBP to a final concentration of 1 mM (50 mins, 25 °C). Rca activities were calculated using the ECM and ER carboxylase time-courses collected on the same day. All assays were performed in assay buffer (100 mM Tricine pH 8.0, 5 mM $MgCl_2$) containing 3 µl coupling enzymes mixture (Creatine P-kinase (2.5 U/ml), Glyceraldehyde-3-P dehydrogenase (2.5 units/ml), 3-phosphoglycerate kinase and Triose-P isomerase/Glycerol-3-P dehydrogenase (20/2 units/ml)), 20 mM $NaHCO_3$, 0.5 mM NADH, 2 mM ATP, 10 mM Creatine-P, 1 mM RuBP. A final concentration of 0.5 µM Rubisco active sites and 2 µM Rca protomer were utilized where appropriate.

ACKNOWLEDGEMENTS

We thank Dr. Manajit Hayer-Hartl for the gift of plasmids pBAD33k-*At*RbcLS, p11a-*At*C60αβ/C20 and pCDFduet-*At*R1/R2/Rx/B2. Lynette Liew synthesized RuBP. pHue*Ath*Rcaβ was cloned by Devendra Shivhare. This work was funded by the Ministry of Education (MOE) of Singapore Tier 2 grant to O.M.-C (MOE2016-T2-2-088).

FIGURE LEGENDS

Figure 1. Production and Rca assay of plant Rubisco variants (*A*) SDS-PAGE analysis of purified recombinant wild-type Arabidopsis Rubisco and βC-βD mutant variants (*B*) Rca functions to remodel inhibited E.R. complexes, releasing RuBP. The apo-enzyme E can then bind non-substrate CO_2 and Mg^{2+} to form the functional E.C.M. holoenzyme. (*C*) Rubisco activation assays of wild type and βC-βD loop mutant Rubisco variants. Assays were performed at 25°C and contained 0.5 μM Rubisco active sites in the presence and absence of Arabidopsis Rca (2 μM protomer). Error bars indicate the S.D. of at least three independent experiments.

Figure 2. Mutational scan of the Rubisco surface (*A*) Mutated surface residues are visualized on the surface of inhibited Arabidopsis Rubisco (PDB: 5IUO) and coloured in groups. (*B*) Electrostatic surface potential as analysed by the Adaptive Poisson-Boltzmann Solver (APBS) wrapper function in PyMOL. The location of a negatively charged patch between two large subunit dimers is circled in yellow. (*C*) Rca function and carboxylation rates of surface mutants in groups corresponding to (*A*). Assays were conducted at 25°C using 0.5 μM Rubisco active sites (ER or ECM) and 2 μM wild type activase protomers when appropriate. Error bars indicate the S.D. of at least three independent experiments. The corresponding time course data is shown in Fig. S2. A significant difference from the wild-type value is indicated by an asterisk (One-way ANOVA, posthoc Tukey test, $p < 0.05$).

Figure 3. The N-terminus of the Rubisco large subunit is essential for Rca function (*A*) Sequence alignment of RbcL N-terminal sequences. In higher plants the N-termini are almost completely conserved, as indicated by a web-logo representation of the consensus sequence (~500 plant RbcL sequences). (*B*) Visualization of the ordered N-terminal segment (yellow- starting from residue 7) using a model of the inhibited *Chlamydomonas reinhardtii* Rubisco (PDB:1GK8). (*C*) Rubisco activase assays of wild-type and ΔN7 mutant Arabidopsis Rubiscos. Assays were conducted at 25°C with 2 μM wild type activase protomers and 0.5 μM Rubisco active sites. Error bars indicate the S.D. of at least three independent experiments.

Figure 4. Mutational analysis of the RbcL N-terminus.

Activase activity and carboxylation rates of Rubisco N-terminal truncations and insertions (*A*) and point mutant (*B*) variants were assayed. Time courses are shown in Fig. S4. Values significantly different from their wild-type equivalent are indicated by an asterisk (One-way ANOVA, posthoc Tukey test, $p < 0.05$).

Figure 5. Model for the Rubisco-Rca interaction. By placing the Helix9 interaction site (in red) of two adjacent Rca subunits in proximity to the βC-βD loops (yellow) of two large subunits belonging to different dimers, the RbcL N-terminus (in magenta- N-terminal 6 amino acids missing) can be positioned under the axial pore of the Rca hexamer. Transient pore-loop threading would then lead to disruptions of interactions between the N-terminus and the catalytic 60s loop, followed by inhibitor release. PDB:1GK8 (Rubisco) and 3ZW6 (Rca). The figure was drawn using ChimeraX (50).

REFERENCES

1. Spreitzer, R. J., and Salvucci, M. E. (2002) Rubisco: structure, regulatory interactions, and possibilities for a better enzyme. *Annual review of plant biology* **53**, 449-475
2. Raven, J. A. (2013) Rubisco: still the most abundant protein of Earth? (vol 198, pg 1, 2013). *New Phytologist* **198**, 970-970
3. Bar-On, Y. M., and Milo, R. (2019) The global mass and average rate of rubisco. *Proc Natl Acad Sci U S A* **116**, 4738-4743
4. Long, S. P., Marshall-Colon, A., and Zhu, X. G. (2015) Meeting the global food demand of the future by engineering crop photosynthesis and yield potential. *Cell* **161**, 56-66
5. Zhu, X. G., Long, S. P., and Ort, D. R. (2010) Improving photosynthetic efficiency for greater yield. *Annual review of plant biology* **61**, 235-261
6. Parry, M. A., Keys, A. J., Madgwick, P. J., Carmo-Silva, A. E., and Andralojc, P. J. (2008) Rubisco regulation: a role for inhibitors. *Journal of experimental botany* **59**, 1569-1580
7. Pearce, F. G., and Andrews, T. J. (2003) The relationship between side reactions and slow inhibition of ribulose-bisphosphate carboxylase revealed by a loop 6 mutant of the tobacco enzyme. *Journal of Biological Chemistry* **278**, 32526-32536
8. Salvucci, M. E., Portis, A. R., Jr., and Ogren, W. L. (1985) A soluble chloroplast protein catalyzes ribulosebisphosphate carboxylase/oxygenase activation in vivo. *Photosynthesis research* **7**, 193-201
9. Tsai, Y. C., Lapina, M. C., Bhushan, S., and Mueller-Cajar, O. (2015) Identification and characterization of multiple rubisco activases in chemoautotrophic bacteria. *Nature communications* **6**, 8883
10. Mueller-Cajar, O., Stotz, M., Wendler, P., Hartl, F. U., Bracher, A., and Hayer-Hartl, M. (2011) Structure and function of the AAA+ protein CbbX, a red-type Rubisco activase. *Nature* **479**, 194-199
11. Mueller-Cajar, O. (2017) The Diverse AAA+ Machines that Repair Inhibited Rubisco Active Sites. *Frontiers in Molecular Biosciences* **4**
12. Hayer-Hartl, M., and Hartl, F. U. (2020) Chaperone Machineries of Rubisco - The Most Abundant Enzyme. *Trends Biochem Sci*
13. Bhat, J. Y., Milicic, G., Thieulin-Pardo, G., Bracher, A., Maxwell, A., Ciniawsky, S., Mueller-Cajar, O., Engen, J. R., Hartl, F. U., Wendler, P., and Hayer-Hartl, M. (2017) Mechanism of Enzyme Repair by the AAA+ Chaperone Rubisco Activase. *Molecular Cell* **67**, 744-756 e746
14. Loganathan, N., Tsai, Y.-C. C., and Mueller-Cajar, O. (2016) Characterization of the heterooligomeric red-type rubisco activase from red algae. *Proceedings of the National Academy of Sciences* **113**, 14019-14024
15. Mueller-Cajar, O., Stotz, M., Wendler, P., Hartl, F. U., Bracher, A., and Hayer-Hartl, M. (2011) Structure and function of the AAA+ protein CbbX, a red-type Rubisco activase. *Nature* **479**, 194-199
16. Tsai, Y. C., Ye, F., Liew, L., Liu, D., Bhushan, S., Gao, Y. G., and Mueller-Cajar, O. (2020) Insights into the mechanism and regulation of the CbbQO-type Rubisco activase, a MoxR AAA+ ATPase. *Proc Natl Acad Sci U S A* **117**, 381-387
17. Bracher, A., Whitney, S. M., Hartl, F. U., and Hayer-Hartl, M. (2017) Biogenesis and Metabolic Maintenance of Rubisco. *Annu Rev Plant Biol* **68**, 29-60
18. Portis, A. R. (2003) Rubisco activase - Rubisco's catalytic chaperone. *Photosynthesis Research* **75**, 11-27
19. Carmo-Silva, E., Scales, J. C., Madgwick, P. J., and Parry, M. A. (2015) Optimizing Rubisco and its regulation for greater resource use efficiency. *Plant, cell & environment* **38**, 1817-1832

20. Stotz, M., Mueller-Cajar, O., Ciniawsky, S., Wendler, P., Hartl, F. U., Bracher, A., and Hayer-Hartl, M. (2011) Structure of green-type Rubisco activase from tobacco. *Nature Structural & Molecular Biology* **18**, 1366-U1378
21. Shivhare, D., Ng, J., Tsai, Y. C., and Mueller-Cajar, O. (2019) Probing the rice Rubisco-Rubisco activase interaction via subunit heterooligomerization. *Proc Natl Acad Sci U S A* **116**, 24041-24048
22. van de Loo, F. J., and Salvucci, M. E. (1996) Activation of ribulose-1,5-bisphosphate carboxylase/oxygenase (Rubisco) involves Rubisco activase Trp16. *Biochemistry* **35**, 8143-8148
23. Wang, Z. Y., Snyder, G. W., Esau, B. D., Portis, A. R., and Ogren, W. L. (1992) Species-Dependent Variation in the Interaction of Substrate-Bound Ribulose-1,5-Bisphosphate Carboxylase Oxygenase (Rubisco) and Rubisco Activase. *Plant physiology* **100**, 1858-1862
24. Larson, E. M., O'Brien, C. M., Zhu, G., Spreitzer, R. J., and Portis, A. R. (1997) Specificity for Activase Is Changed by a Pro-89 to Arg Substitution in the Large Subunit of Ribulose-1,5-bisphosphate Carboxylase/Oxygenase. *Journal of Biological Chemistry* **272**, 17033-17037
25. Aigner, H., Wilson, R. H., Bracher, A., Calisse, L., Bhat, J. Y., Hartl, F. U., and Hayer-Hartl, M. (2017) Plant RuBisCo assembly in E. coli with five chloroplast chaperones including BSD2. *Science* **358**, 1272-1278
26. Wilson, R. H., Thieulin-Pardo, G., Hartl, F. U., and Hayer-Hartl, M. (2019) Improved recombinant expression and purification of functional plant Rubisco. *FEBS Lett* **593**, 611-621
27. Ott, C. M., Smith, B. D., Portis, A. R., Jr., and Spreitzer, R. J. (2000) Activase Region on Chloroplast Ribulose-1,5-bisphosphate Carboxylase/Oxygenase. NONCONSERVATIVE SUBSTITUTION IN THE LARGE SUBUNIT ALTERS SPECIES SPECIFICITY OF PROTEIN INTERACTION

10.1074/jbc.M004580200. *J. Biol. Chem.* **275**, 26241-26244
28. Shivhare, D., and Mueller-Cajar, O. (2017) Characterization of thermostable CAM Rubisco activase reveals a Rubisco interacting surface loop. *Plant Physiology*
29. Wang, H., Yan, X., Aigner, H., Bracher, A., Nguyen, N. D., Hee, W. Y., Long, B. M., Price, G. D., Hartl, F. U., and Hayer-Hartl, M. (2019) Rubisco condensate formation by CcmM in beta-carboxysome biogenesis. *Nature* **566**, 131-135
30. Oltrogge, L. M., Chaijarasphong, T., Chen, A. W., Bolin, E. R., Marqusee, S., and Savage, D. F. (2020) Multivalent interactions between CsoS2 and Rubisco mediate alpha-carboxysome formation. *Nat Struct Mol Biol* **27**, 281-287
31. Satagopan, S., and Spreitzer, R. J. (2004) Substitutions at the Asp-473 Latch Residue of Chlamydomonas Ribulosebisphosphate Carboxylase/Oxygenase Cause Decreases in Carboxylation Efficiency and CO2/O2 Specificity

10.1074/jbc.M313215200. *J. Biol. Chem.* **279**, 14240-14244
32. Schreuder, H. A., Knight, S., Curmi, P. M. G., Andersson, I., Cascio, D., Branden, C. I., and Eisenberg, D. (1993) Formation of the Active-Site of Ribulose-1,5-Bisphosphate Carboxylase Oxygenase by a Disorder Order Transition from the Unactivated to the Activated Form. *Proceedings of the National Academy of Sciences of the United States of America* **90**, 9968-9972
33. Gutteridge, S., Millard, B. N., and Parry, M. A. J. (1986) Inactivation of ribulose-bisphosphate carboxylase by limited proteolysis. *FEBS Letters* **196**, 263-268
34. Puchades, C., Rampello, A. J., Shin, M., Giuliano, C. J., Wiseman, R. L., Glynn, S. E., and Lander, G. C. (2017) Structure of the mitochondrial inner membrane AAA+ protease YME1 gives insight into substrate processing. *Science* **358**
35. Shin, M., Puchades, C., Asmita, A., Puri, N., Adjei, E., Wiseman, R. L., Karzai, A. W., and Lander, G. C. (2020) Structural basis for distinct operational modes and protease activation in AAA+ protease Lon. *Science Advances* **6**, eaba8404

383 36. Gates, S. N., Yokom, A. L., Lin, J., Jackrel, M. E., Rizo, A. N., Kendsersky, N. M., Buell, C. E.,
384 Sweeny, E. A., Mack, K. L., Chuang, E., Torrente, M. P., Su, M., Shorter, J., and Southworth, D.
385 R. (2017) Ratchet-like polypeptide translocation mechanism of the AAA+ disaggregase
386 Hsp104. *Science* **357**, 273-279
387 37. Han, H., Monroe, N., Sundquist, W. I., Shen, P. S., and Hill, C. P. (2017) The AAA ATPase Vps4
388 binds ESCRT-III substrates through a repeating array of dipeptide-binding pockets. *Elife* **6**
389 38. Yu, H., Lupoli, T. J., Kovach, A., Meng, X., Zhao, G., Nathan, C. F., and Li, H. (2018) ATP
390 hydrolysis-coupled peptide translocation mechanism of Mycobacterium tuberculosis ClpB.
391 *Proc Natl Acad Sci U S A* **115**, E9560-E9569
392 39. Parry, M. A. J., Andralojc, P. J., Mitchell, R. A. C., Madgwick, P. J., and Keys, A. J. (2003)
393 Manipulation of Rubisco: the amount, activity, function and regulation. *Journal of*
394 *Experimental Botany* **54**, 1321-1333
395 40. Mueller-Cajar, O., and Whitney, S. M. (2008) Evolving improved Synechococcus Rubisco
396 functional expression in Escherichia coli. *Biochem J* **414**, 205-214
397 41. Wilson, R. H., Martin-Avila, E., Conlan, C., and Whitney, S. M. (2018) An improved
398 Escherichia coli screen for Rubisco identifies a protein-protein interface that can enhance
399 CO2-fixation kinetics. *J Biol Chem* **293**, 18-27
400 42. Puchades, C., Sandate, C. R., and Lander, G. C. (2020) The molecular principles governing the
401 activity and functional diversity of AAA+ proteins. *Nat Rev Mol Cell Biol* **21**, 43-58
402 43. Portis, A. R., Li, C. S., Wang, D. F., and Salvucci, M. E. (2008) Regulation of Rubisco activase
403 and its interaction with Rubisco. *Journal of Experimental Botany* **59**, 1597-1604
404 44. Larson, E. M., O'Brien, C. M., Zhu, G., Spreitzer, R. J., and Portis Jr., A. R. (1997) Specificity for
405 Activase Is Changed by a Pro-89 to Arg Substitution in the Large Subunit of Ribulose-1,5-
406 bisphosphate Carboxylase/Oxygenase

407 10.1074/jbc.272.27.17033. *J. Biol. Chem.* **272**, 17033-17037
408 45. Taylor, T. C., Backlund, A., Bjorhall, K., Spreitzer, R. J., and Andersson, I. (2001) First crystal
409 structure of rubisco from a green alga, Chlamydomonas reinhardtii. *Journal of Biological*
410 *Chemistry* **276**, 48159-48164
411 46. Flecken, M., Wang, H., Popilka, L., Hartl, F. U., Bracher, A., and Hayer-Hartl, M. (2020) Dual
412 Role of a Rubisco Activase in Metabolic Repair and Carboxysome Organization. *bioRxiv*,
413 2020.2005.2016.099382
414 47. Kubien, D. S., Brown, C. M., and Kane, H. J. (2011) Quantifying the amount and activity of
415 Rubisco in leaves. *Methods in molecular biology* **684**, 349-362
416 48. Horecker, B. L., Hurwitz, J., and Weissbach, A. (1958) Ribulose diphosphate. *Biochemical*
417 *Preparations* **6**, 83-90
418 49. Kane, H. J., Wilkin, J. M., Portis, A. R., and Andrews, T. J. (1998) Potent inhibition of ribulose-
419 bisphosphate carboxylase by an oxidized impurity in ribulose-1,5-bisphosphate. *Plant*
420 *Physiology* **117**, 1059-1069
421 50. Goddard, T. D., Huang, C. C., Meng, E. C., Pettersen, E. F., Couch, G. S., Morris, J. H., and
422 Ferrin, T. E. (2018) UCSF ChimeraX: Meeting modern challenges in visualization and analysis.
423 *Protein Sci* **27**, 14-25

424

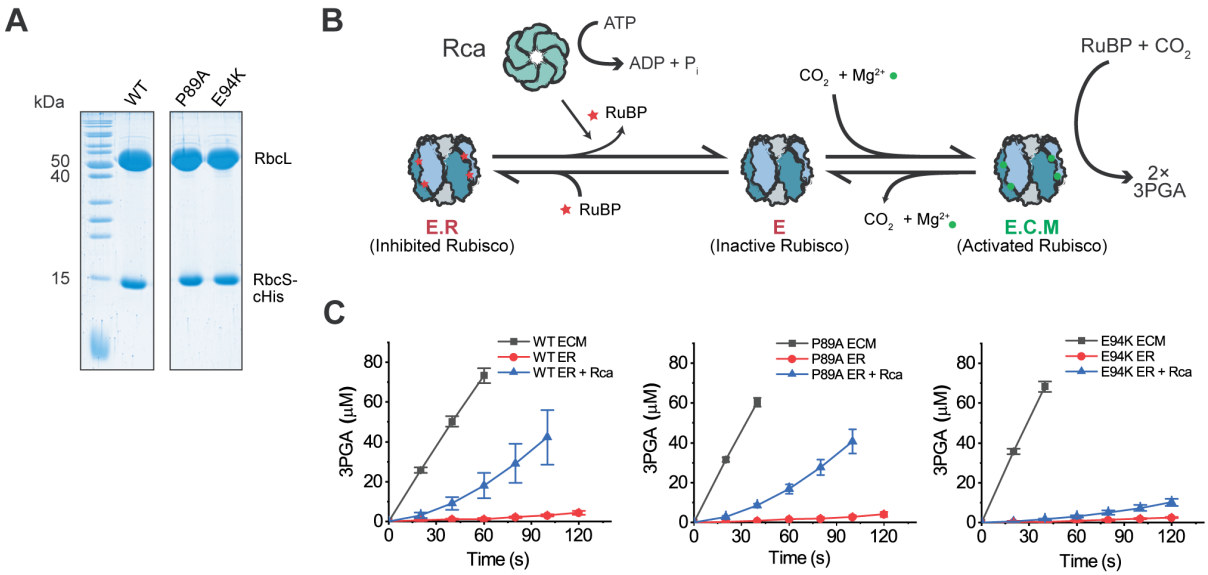

Figure 1. Production and Rca assay of plant Rubisco variants (*A*) SDS-PAGE analysis of purified recombinant wild-type Arabidopsis Rubisco and βC-βD mutant variants (*B*) Rca functions to remodel inhibited E.R. complexes, releasing RuBP. The apo-enzyme E can then bind non-substrate CO_2 and Mg^{2+} to form the functional E.C.M. holoenzyme. (*C*) Rubisco activation assays of wild type and βC-βD loop mutant Rubisco variants. Assays were performed at 25°C and contained 0.5 μM Rubisco active sites in the presence and absence of Arabidopsis Rca (2 μM protomer). Error bars indicate the S.D. of at least three independent experiments.

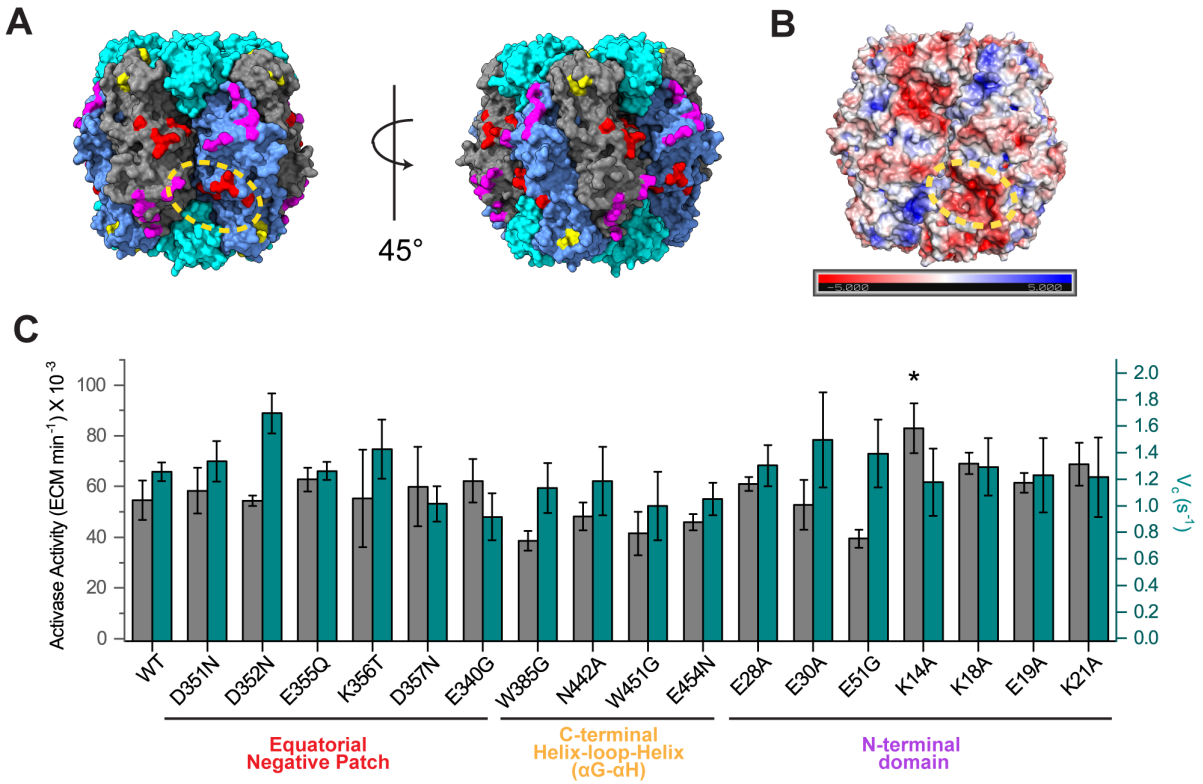

Figure 2. Mutational scan of the Rubisco surface (*A*) Mutated surface residues are visualized on the surface of inhibited Arabidopsis rubisco (PDB: 5IUO) and coloured in groups. (*B*) Electrostatic surface potential as analysed by the Adaptive Poisson-Boltzmann Solver (APBS) wrapper function in PyMOL. The location of a negatively charged patch between two large subunit dimers is circled in yellow. (*C*) Rca function and carboxylation rates of surface mutants in groups corresponding to (*A*). Assays were conducted at 25°C using 0.5 μM Rubisco active sites (ER or ECM) and 2 μM wild type activase protomers when appropriate. Error bars indicate the S.D. of at least three independent experiments. The corresponding time course data is shown in Fig. S2. A significant difference from the wild-type value is indicated by an asterisk (One-way ANOVA, posthoc Tukey test, $p < 0.05$).

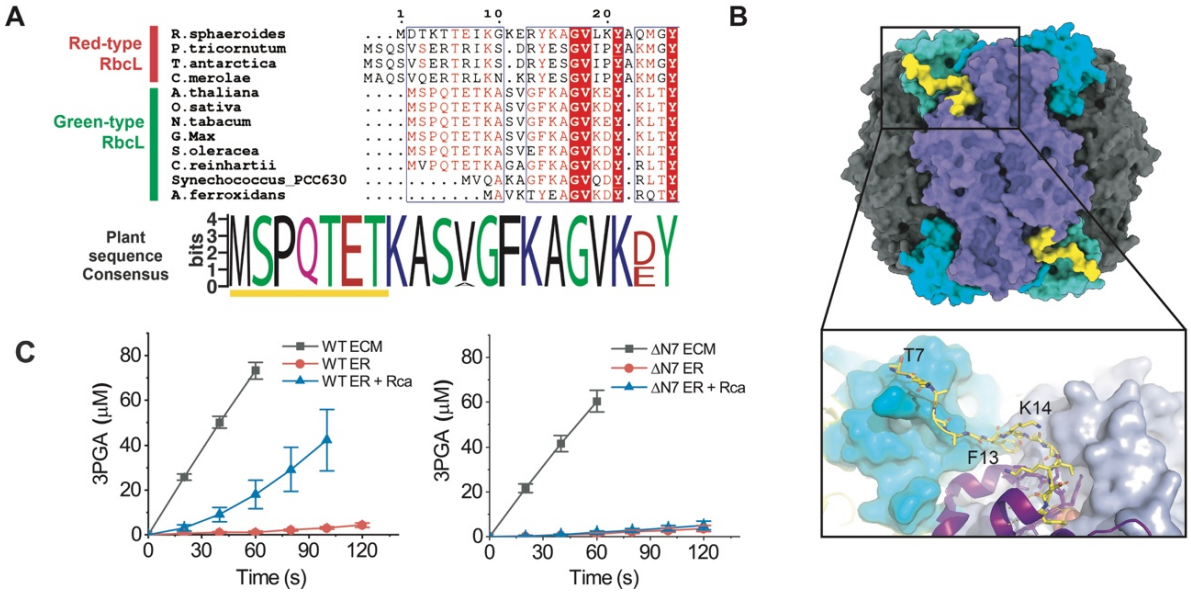

Figure 3. The N-terminus of the Rubisco large subunit is essential for Rca function (*A*) Sequence alignment of RbcL N-terminal sequences. In higher plants the N-termini are almost completely conserved, as indicated by a web-logo representation of the consensus sequence (~500 plant RbcL sequences). (*B*) Visualization of the ordered N-terminal segment (yellow-starting from residue 7) using a model of the inhibited *Chlamydomonas reinhardtii* Rubisco (PDB:1GK8). (*C*) Rubisco activase assays of wild-type and ΔN7 mutant Arabidopsis Rubiscos. Assays were conducted at 25°C with 2μM wild type activase protomers and 0.5 μM Rubisco active sites. Error bars indicate the S.D. of at least three independent experiments.

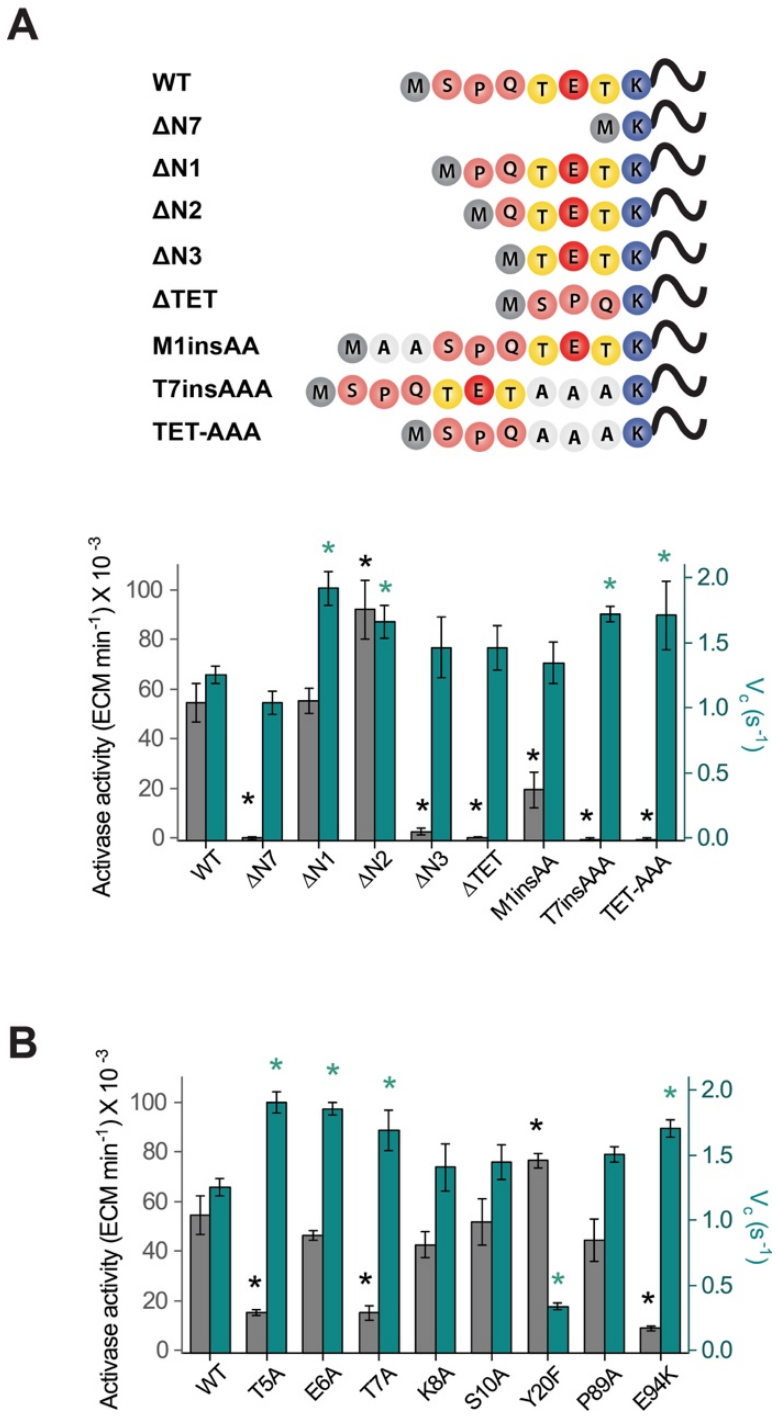

Figure 4. Mutational analysis of the RbcL N-terminus.
Activase activity and carboxylation rates of Rubisco N-terminal truncations and insertions (*A*) and point mutant (*B*) variants were assayed. Time courses are shown in Fig. S4. Values significantly different from their wild-type equivalent are indicated by an asterisk (One-way ANOVA, posthoc Tukey test, $p < 0.05$).

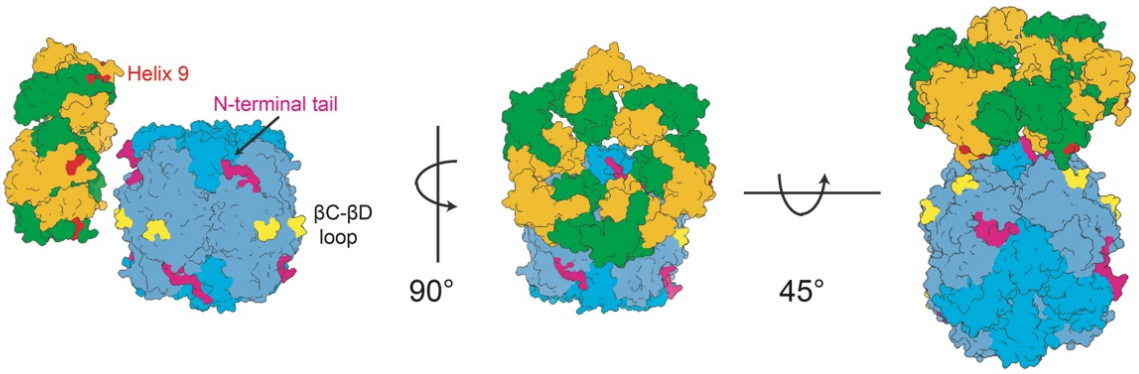

Figure 5. Model for the Rubisco-Rca interaction. By placing the Helix 9 interaction site (in red) of two adjacent Rca subunits in proximity to the βC-βD loops (yellow) of two large subunits belonging to different dimers, the RbcL N-terminus (in magenta- N-terminal 6 amino acids missing) can be positioned under the axial pore of the Rca hexamer. Transient pore-loop threading would then lead to disruptions of interactions between the N-terminus and the catalytic 60s loop, followed by inhibitor release. PDB:1GK8 (Rubisco) and 3ZW6 (Rca).

Supporting Information (SI)

Rubisco activase remodels plant Rubisco via the large subunit N-terminus

Jediael Ng and Oliver Mueller-Cajar*

School of Biological Sciences, Nanyang Technological University, 60 Nanyang Drive,

Singapore 637551. Singapore

*Correspondence: cajar@ntu.edu.sg

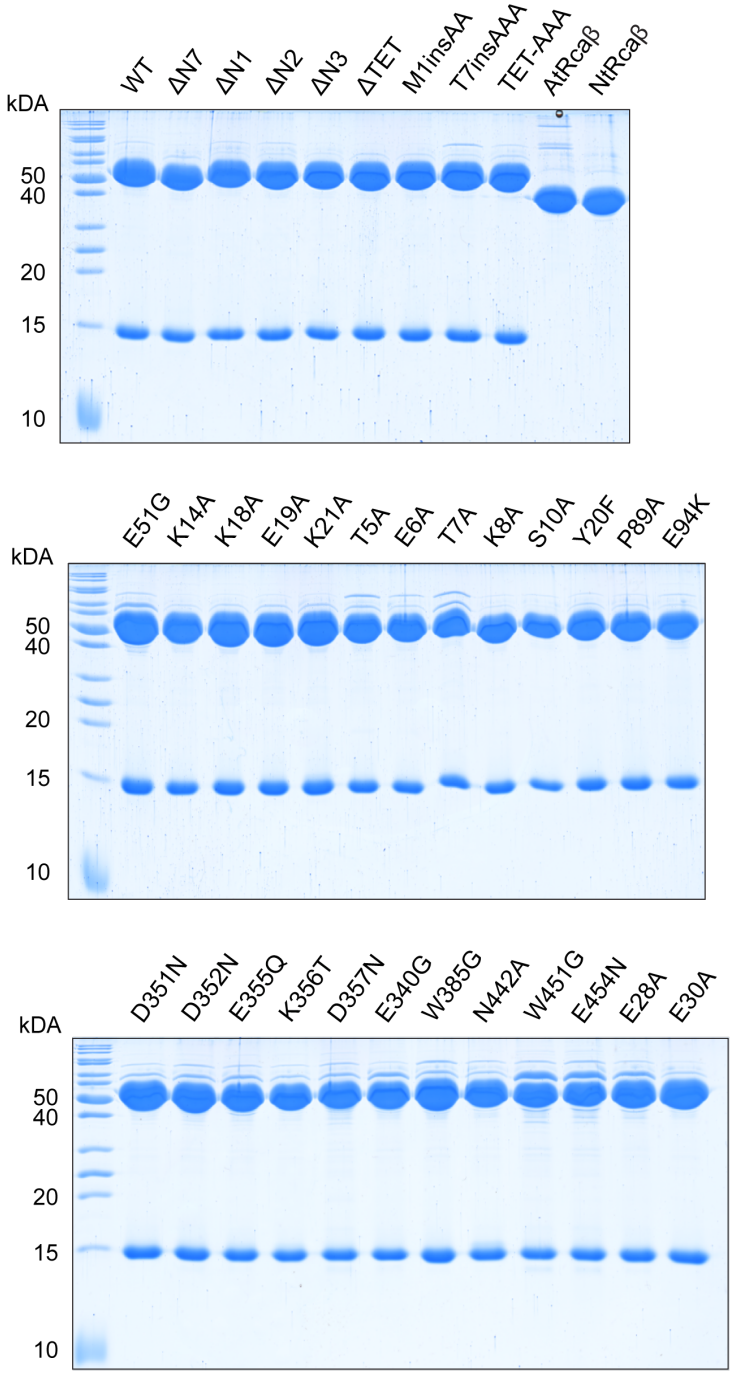

Fig. S1. SDS-PAGE analysis of proteins used in this study. 4 µg of purified protein was loaded per lane.

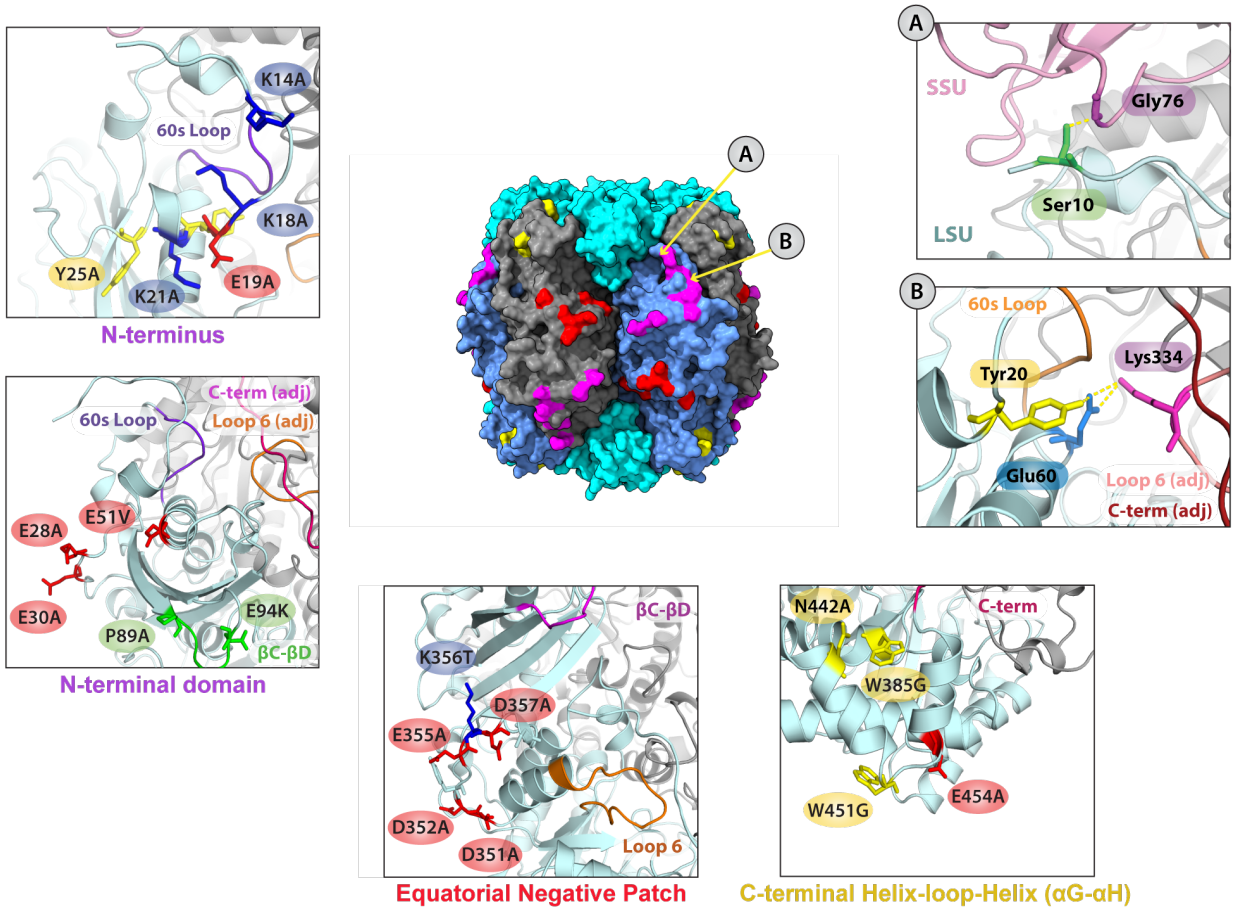

Fig. S2. Structural representations of mutated residues on the surface of Rubisco. Detailed views of surface residues substituted in the mutational analysis. Panels on the right depict the interaction network for S10 and Y20. Serine 10 hydrogen bonds to Glycine 67 of the small subunit while the hydroxyl group on the side chain of Tyrosine 20 hydrogen bonds to Glutamate 60. Mutants of these residues were generated to investigate whether these interactions were essential for the mechanism of the activase (Fig. 4*B*).

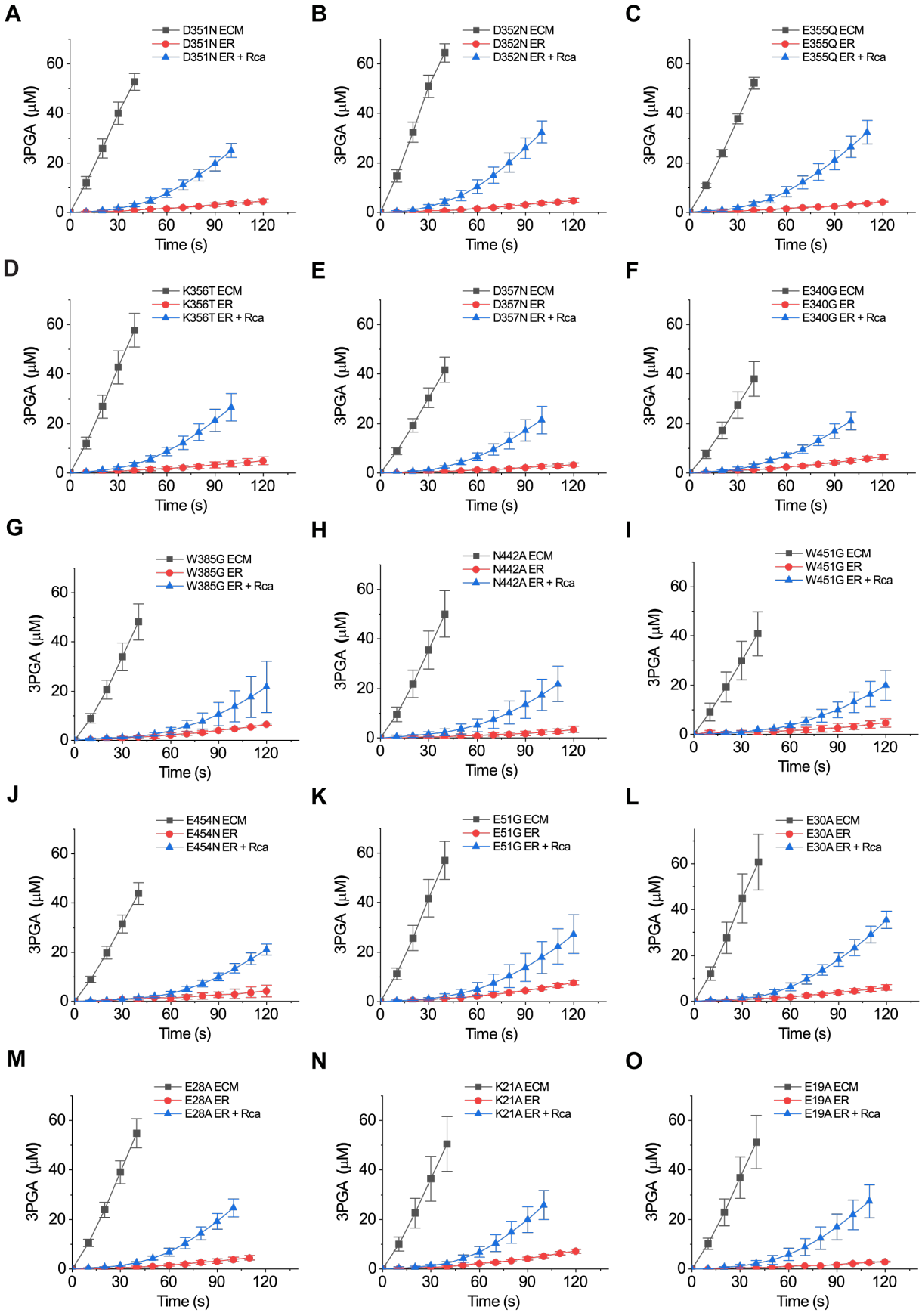
A
D351N ECM
D351N ER
D351N ER + Rca
B
D352N ECM
D352N ER
D352N ER + Rca
C
E355Q ECM
E355Q ER
E355Q ER + Rca
D
K356T ECM
K356T ER
K356T ER + Rca
E
D357N ECM
D357N ER
D357N ER + Rca
F
E340G ECM
E340G ER
E340G ER + Rca
G
W385G ECM
W385G ER
W385G ER + Rca
H
N442A ECM
N442A ER
N442A ER + Rca
I
W451G ECM
W451G ER
W451G ER + Rca
J
E454N ECM
E454N ER
E454N ER + Rca
K
E51G ECM
E51G ER
E51G ER + Rca
L
E30A ECM
E30A ER
E30A ER + Rca
M
E28A ECM
E28A ER
E28A ER + Rca
N
K21A ECM
K21A ER
K21A ER + Rca
O
E19A ECM
E19A ER
E19A ER + Rca
3PGA (μM)
Time (s)
0
20
40
60
0
30
60
90
120

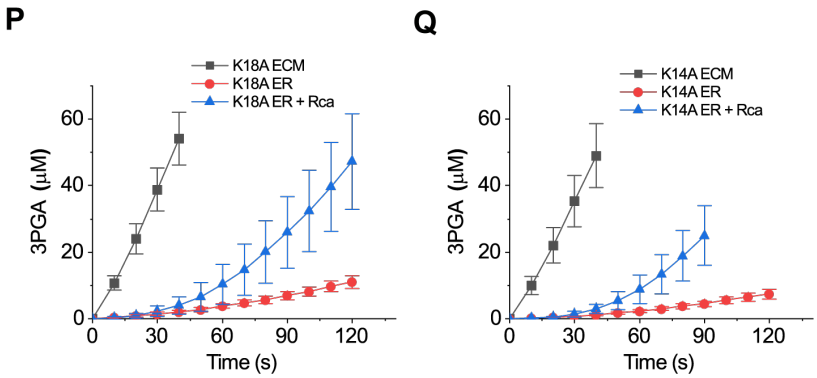

Fig. S3. Rubisco activase assays of surface mutant variants. Carboxylation time course data of activated Rubisco (ECM), inhibited Rubisco (ER), and inhibited Rubisco in the presence of wild type Arabidopsis activase (*At*Rcaβ) is shown for all mutants described in Fig. 2C.

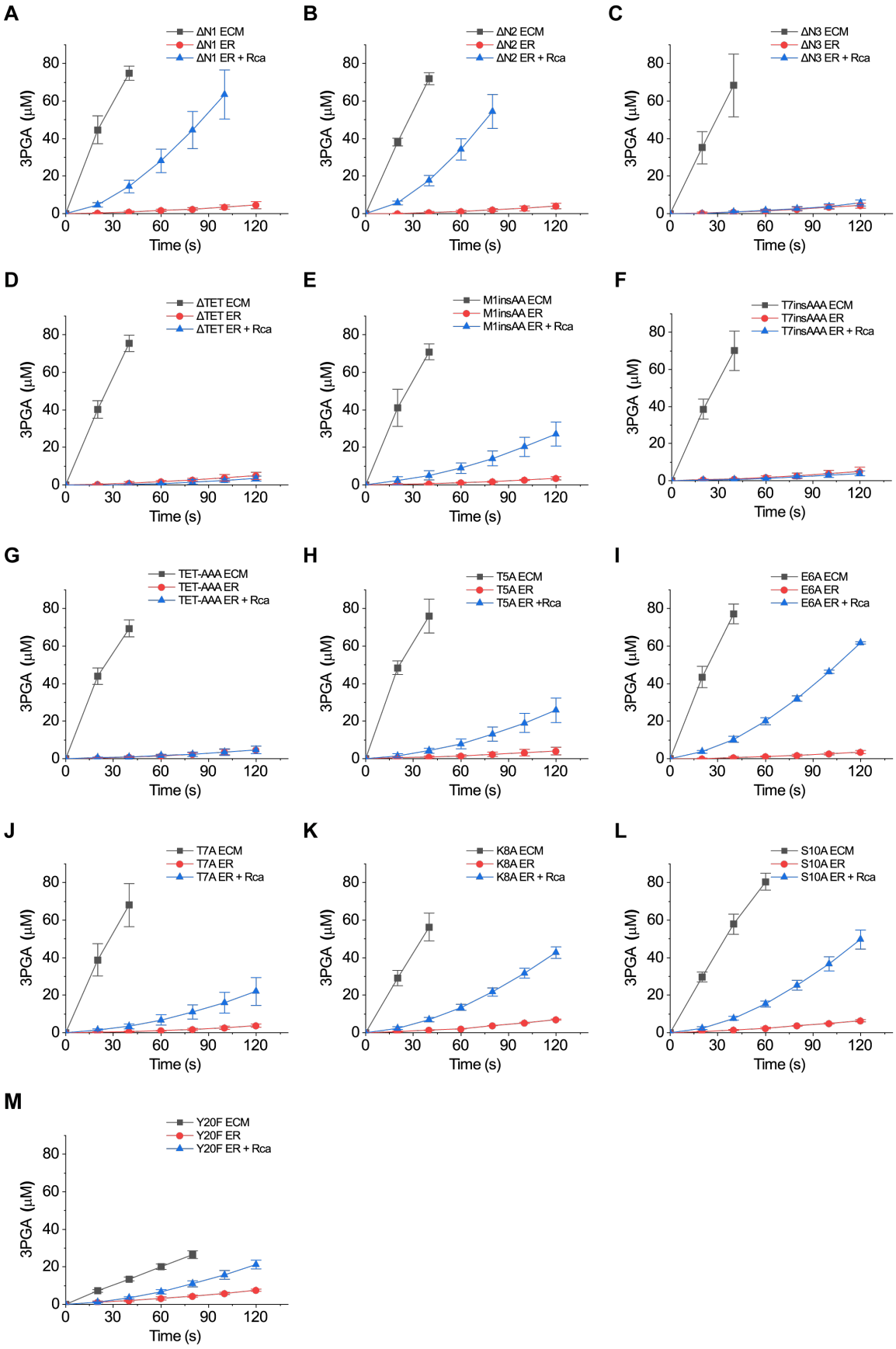
A
ΔN1 ECM
ΔN1 ER
ΔN1 ER + Rca
B
ΔN2 ECM
ΔN2 ER
ΔN2 ER + Rca
C
ΔN3 ECM
ΔN3 ER
ΔN3 ER + Rca
D
ΔTET ECM
ΔTET ER
ΔTET ER + Rca
E
M1insAA ECM
M1insAA ER
M1insAA ER + Rca
F
T7insAAA ECM
T7insAAA ER
T7insAAA ER + Rca
G
TET-AAA ECM
TET-AAA ER
TET-AAA ER + Rca
H
T5A ECM
T5A ER
T5A ER +Rca
I
E6A ECM
E6A ER
E6A ER + Rca
J
T7A ECM
T7A ER
T7A ER + Rca
K
K8A ECM
K8A ER
K8A ER + Rca
L
S10A ECM
S10A ER
S10A ER + Rca
M
Y20F ECM
Y20F ER
Y20F ER + Rca
3PGA (μM)
Time (s)
0
20
40
60
80
0
30
60
90
120

Fig. S4. Rubisco activase assays of N-terminal mutant variants. Carboxylation time course data of activated Rubisco (ECM), inhibited Rubisco (ER), and inhibited Rubisco in the presence of wild type Arabidopsis activase (*At*Rcaβ) are shown for all mutants described in Fig. 4*A*-*B*.

Table S1. Primers used in this study

No.	Primer	Sequence (5' to 3')
1	AtHLS E94K for	CCGTTCCAGGAGAAAAGACTCAATTTATTGC
2	AtHLS E94K rev	GCAATAAATTGAGTCTTTTCTCCTGGAACGG
3	AtHLS P89A for	TGCTACCACATCGAGGCCGTTCCAGGAGAA
4	AtHLS P89A rev	TTCTCCTGGAACGGCCTCGATGTGGTAGCA
5	AtHLS E51V for	GAGTTCCACCTGTAGAAGCAGGGGC
6	AtHLS E51V rev	GCCCCTGCTTCTACAGGTGGAACTC
7	AtHLS E28A for	GACTTACTATACTCCTGCATATGAAACCAAGG
8	AtHLS E28A rev	CCTTGGTTTCATATGCAGGAGTATAGTAAGTC
9	AtHLS E30A for	ACTCCTGAATATGCAACCAAGGATACTG
10	AtHLS E30A rev	CAGTATCCTTGGTTGCATATTCAGGAGT
11	AtHLS ΔN7 dp for	AAAGCAAGTGTTGGGTTCAAAGCTGGT
12	AtHLS ΔN7 dp rev	CATATGTATATCTCCTTCTTAAAGTTAAACAAAATTATT TCTAGAGGG
13	AtHLS ΔN4 dp for (used with 12)	ACAGAGACTAAAGCAAGTGTTGGGT
14	AtHLS NinsAA dp for (used with 12)	GCTGCATCACCACAAACAGAGACTAAAGCAAG
15	AtHLS ΔTET rev (used with 11)	TTGTGGTGACATATGTATATCTCCTTCTTAAAGTTAAAC AAAATTATTTCTAGAG
16	AtHLS ΔN2 dp for (used with 12)	CAAACAGAGACTAAAGCAAGTGTTGGG
17	AtHLS ΔN1 dp for (used with 12)	CCACAAACAGAGACTAAAGCAAGTGTTG
18	AtHLS TETAAA dp for	AGCTAAAGCAAGTGTTGGGT
19	AtHLS TETAAA dp rev	GCAGCTTGTGGTGACATATGTATATCTC
20	AtHLS 8insAAA dp for	GCAGCAGTCTCTGTTTGTGGTGACAT
21	AtHLS 8insAAA dp rev	AGCTAAAGCAAGTGTTGGGTTCAAAG
22	AtHLS T5A for	ATATGTCACCACAAGCAGAGACTAAAGCAAG
23	AtHLS T5A rev	CTTGCTTTAGTCTCTGCTTGTGGTGACATAT

24	AtHLS E6A for	GTCACCACAAACAGCAACTAAAGCAAGTGTTG
25	AtHLS E6A rev	CAACACTTGCTTTAGTTGCTGTTTGTGGTGAC
26	AtHLS T7A for	GTCACCACAAACAGAGGCTAAAGCAAGTGTTG
27	AtHLS T7A rev	CAACACTTGCTTTAGCCTCTGTTTGTGGTGAC
28	AtHLS K8A for	CACAAACAGAGACTGCAGCAAGTGTTGGGTTC
29	AtHLS K8A rev	GAACCCAACACTTGCTGCAGTCTCTGTTTGTG
30	AtHLS S10A for	CAGAGACTAAAGCAGCAGTTGGGTTCAAAGCTG
31	AtHLS S10A rev	CAGCTTTGAACCCAACTGCTGCTTTAGTCTCTG
32	AtHLS Y20F for	GCTGGTGTTAAAGAGTTTAAATTGACTTACTATACTCC
33	AtHLS Y20F rev	GGAGTATAGTAAGTCAATTTAAACTCTTTAACACCAGC
34	AtHLS Region1 for	TAAACTTGAAGGAGACGCGGCGTCAACTTTGGGCTTTG
35	AtHLS Region1 rev	CAAAGCCCAAAGTTGACGCCGCGTCTCCTTCAAGTTTA
36	AtHLS Region2 for	GCTTTGTTGATTTACTGCTCGCTGCTTCTGTTGAAAAAG ATCGAAGC
37	AtHLS Region2 Rev	GCTTCGATCTTTTTCAACAGAAGCAGCGAGCAGTAAAT CAACAAAGC
38	AtHLS Region3 for	GCGATGATTATGTTGCAAAAGCTCGAAGCCGCGGTATC
39	AtHLS Region3 Rev	GATACCGCGGCTTCGAGCTTTTGCAACATAATCATCGC
40	AtHLS Region4 for	CATGCCTGCTTTGACCGCGATCTTAGGAGATGATTCTGT AC
41	AtHLS Region4 Rev	GTACAGAATCATCTCCTAAGATCGCGGTCAAAGCAGGC ATG
42	AtHRcaS E454N for	CTTGCAAATGGAGTCCTCAACTAGCTGCTGCTTG
43	AtHRcaS E454N rev	CAAGCAGCAGCTAGTTGAGGACTCCATTTGCAAG
44	AtHLS D357N for	GATTATGTTGAAAAAAATCGAAGCCGCGG
45	AtHLS D357N rev	CCGCGGCTTCGATTTTTTTCAACATAATC
46	AtHLS E355Q for	GCGATGATTATGTTCAAAAAGATCGAAGCCG
47	AtHLS E355Q rev	CGGCTTCGATCTTTTTGAACATAATCATCGC
48	AtHLS D352N for	GTTGATTTACTGCGCGATAATTATGTTGAAAAAGATCG

49	AtHLS D352N rev	CGATCTTTTTCAACATAATTATCGCGCAGTAAATCAAC
50	AtHLS D351N for	GCTTTGTTGATTTACTGCGCAATGATTATGTTGAAAAAG ATC
51	AtHLS D351N rev	GATCTTTTTCAACATAATCATTGCGCAGTAAATCAACAA AGC
52	AtHLS E340G for	GAAGGAGACAGGGGGTCAACTTTGGG
53	AtHLS E340G rev	CCCAAAGTTGACCCCCTGTCTCCTTC
54	AtHLS E454N for	AAATGGAGTCCTCAACTAGCTGCTG
55	AtHLS E454N rev	CAGCAGCTAGTTGAGGACTCCATTT
56	AtHLS W385G for	GGGTATTCACGTTGGGCACATGCCTGCT
57	AtHLS W385G rev	AGCAGGCATGTGCCCAACGTGAATACCC
58	AtHLS N442A for	GATCTTGCAGTCGAGGGTGCAGAAATTATCCGTGAAGC
59	AtHLS N442A rev	GCTTCACGGATAATTTCTGCACCCTCGACTGCAAGATC
60	AtHLS W451A for	CGTGAAGCTTGCAAAGCAAGTCCTGAACTAGCT
61	AtHLS W451A rev	AGCTAGTTCAGGACTTGCTTTGCAAGCTTCACG